Channel Characterization for Power Line Communication in a Hybrid Electric Vehicle

Nima Taherinejad, Roberto Rosales, Lutz Lampe and Shahriar Mirabbasi
Department of Electrical Engineering and Computer Engineering
University of British Columbia, Vancouver, British Columbia
{nimat, robertor, lampe, shahriar}@ece.ubc.ca

***Abstract*—In today's electric and conventional combustion engine vehicles, data communication between electronic control units is accomplished by sending communication signals over dedicated wires. The space requirement, weight, and installation costs for these wires can become significant, especially in electric vehicles (EVs) of the future, which are highly sophisticated electronic systems. The concept of reusing existing electricity wires, which are needed to power electronic components, for data communication, i.e., vehicular power line communications (V-PLC), is thus a promising means to reduce the amount of dedicated wiring and/or establish redundant communication buses especially for EVs. Previous work on V-PLC has mostly focused on combustion engine vehicles. In this paper, we present the methodology and results from a measurement campaign with the goal of characterizing the transmission conditions for V-PLC in a hybrid EV (HEV). Emphasis is given to the choice of measurement points (potential nodes of a V-PLC network) and the proper design of adapters for measurement equipment. The results presented here focus on channel transfer function and access impedance.**

I. Introduction

Electronics has become one of the most important components in modern vehicles, with forecasts predicting that some 2 billion nodes per year will be connected in car electronic networks by 2014 [1]. This trend also indicates the need for efficient automotive communication networking to accommodate the intra-vehicle information flow. Since usually every network node that communicates is connected to the low-voltage DC power supply of the vehicle, power line communications (PLC) [2] becomes an interesting option for inter-vehicular communications. In particular, the promises of vehicular PLC (V-PLC) would be reduction in cost, use of space, and weight of the wiring harness, as well as fast installation and easy retrofitting. These advantages are even more pronounced in electric vehicles (EVs), since compared to conventional internal combustion engine (ICE) vehicles, additional communication for power and battery management is required. While PLC can replace wires, it can also be used as an independent and redundant communication bus, without any wiring overhead, to reduce failure risks and support "X-by-wire" concepts.

This work was supported by the AUTO21 Network of Centres of Excellence and the National Sciences and Engineering Research Council (NSERC) of Canada.

V-PLC, especially for cars, is not a new concept and some early works include, for example, [3]–[5]. Furthermore, there is a sizeable body of recent literature reporting measurement results for transmission and noise characterization for V-PLC, e.g., [6]–[12]. The literature on V-PLC for EVs, however, is sparse. Barmada et al. [13] present results from a measurement campaign on a fully electric vehicle, namely a Piaggio Porter, and Bassi et al. [14] discuss requirements of V-PLC for EVs and show preliminary laboratory measurement results using proprietory DCB500 transceivers [15].

Considering that the proper characterization and possible understanding of the transmission channel is a necessary first step towards the design and deployment of V-PLC systems, with this work we wish to contribute to the available knowledge base on channel characterization for V-PLC in EVs. More specifically, in this paper we present the methodology and results of a measurement campaign using a hybrid EV (HEV) built on a Ford E-450 cutaway chassis truck and using the Balance^{TM}Hybrid Electric drive system by Azure Dynamics Corporation (AZD). A version of this vehicle has been made available to us by AZD, providing access to internal nodes that would be of interest for a V-PLC system. We have also been able to operate the vehicle in different states, including activated ICE and electrical drive system.

With regards to the former, the results indicate distance-dependent attenuation and changes when the electrical drive system is activated. The access impedances are found to vary widely for different node locations and to exhibit different frequency-selective behaviour. The measurement results can be downloaded at http://www.ece.ubc.ca/~lampe/VehiclePLC_folder/PLC.htm.

The details about the vehicle and measurement methodology are given in Section II. We then present and discuss a number of measurement results for channel transfer function and access impedance in Section III. Finally, Section IV concludes the paper.

II. Measurement Setup

In this section, we first describe the HEV available for measurements. We then explain in detail the applied methodology, which is critical to obtain useful and correct results.

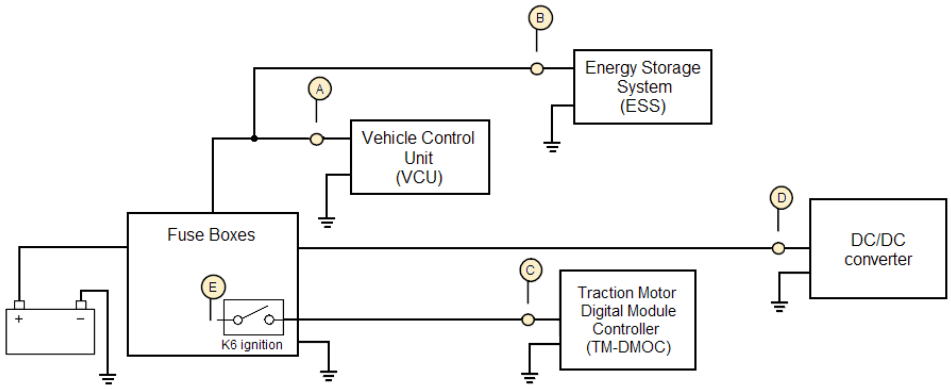

Fig. 1: Electric diagram of the selected access points and their connection to the 12V battery.

A. Vehicle

The vehicle employed for this measurement campaign is an Azure Dynamics Balance^{TM}Hybrid Electric. This vehicle is built on a Ford E-450 cutaway chassis truck, and transformed into an HEV by the addition of proprietary electric drivetrain technology and a high voltage Lithium-Ion battery. The body of the vehicle is thereafter built for different roles, such as passenger shuttle or delivery truck. As an HEV the unit combines its automatic transmission with a conventional combustion engine and an electric traction motor. The combustion engine is used to run the vehicle at speeds above 35 mph (56 kmph) or when the high voltage battery needs recharging. The electric traction is used to run the vehicle at speeds below 35 mph, to assist the combustion engine when accelerating, and to harvest energy from regenerative braking events [16], [17]. Finally, it is worth mentioning that the Azure Dynamics Balance^{TM}Hybrid Electric is available in both a single or dual 12V battery option, and a single or dual DC/DC converter option. The results presented in this work are for a single battery, single DC/DC converter vehicle.

B. Methodology

Next, we provide details of the experimental setup and an overview of all the measurements performed.

1) Access Point: For the selection of the measurement nodes the following criteria were used: a) proximity to the Controller Area Network (CAN) buses, b) proximity to main HEV blocks, and c) availability of connectors with both wiring to "VBAT" (12V battery positive terminal) and "CHASSIS_GND" (12V battery negative terminal through vehicle body). The measurements were performed on an engineering prototype version of the vehicle, stripped of the body and all its components other than the driver seat, steering column and wheel, accelerator, brakes, and instrument panel. The lack of body allowed us to gain easier access to the nodes of interest, but eliminates the possibility of the chassis body acting as signal return path. However, since all test nodes were selected at cable bundles with wiring for both "VBAT" and "CHASSIS_GND", the return path is provided by the connection of the "CHASSIS_GND" wiring to the internal metal body of the vehicle.

The access points selected are the Vehicle Control Unit (VCU), the Energy Storage System (ESS), the Traction Motor Digital Module Controller (TMDMOC), the DC/DC converter, and the relay "K6" in a central fuse box. These are potential nodes in a PLC network. Their roles in the HEV are as follows (cf. [16], [17]).

A) The VCU controls and coordinates the operation of all hybrid components. For example when in electric mode, it is responsible for shutting down the combustion engine and decoupling the engine from the drive wheels.
B) The ESS is a 345V Lithium-Ion battery used to drive the vehicle in electric mode, capture regenerative braking energy, and assist the engine during vehicle acceleration.
C) The TMDMOC converts the high DC voltage from the ESS to 3-phase AC when driving the electric traction motor, or can also perform the opposite power conversion during regenerative braking events to store energy in the ESS. It also controls the speed and torque of the traction motor. The TMDMOC is connected to VBAT upon ignition via the relay K6 as shown in Figure 1
D) The DC/DC converter is used to convert the high DC voltage from the ESS to 12V DC, in order to charge the 12V battery and power 12V electrical accessories.
E) The relay K6 is located in the low-voltage under-the-hood fuse box and provides 12V power to the TMDMOC upon ignition. It should be noted that to access this node we need to remove the relay, therefore measurements from the relay access point to other nodes are not possible with engines running.

Figure 1 shows an electric diagram of the selected access points and their connection to the 12V battery. Complete electric diagrams for this vehicle are available online, see [18].

TABLE I: Ports at which VNA measurements were performed. Vehicle state: O=off, IG=ignition, ID=idle, S=wheels spinning.

	VCU	ESS	TMDMOC	DC/DC	Relay
VCU		O,IG,ID	O,IG,ID	O,IG,ID,S	O,IG
ESS			O,IG,ID	O,IG,ID,S	O,IG
TMDMOC				O,IG,ID,S	O,IG
DC/DC					O,IG
Relay					

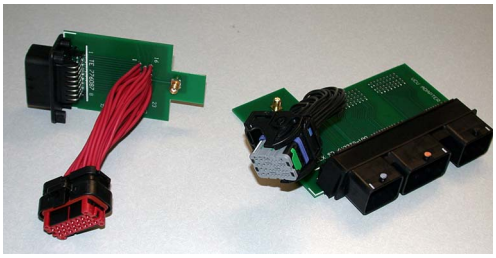

Fig. 2: Adapters for channel measurements. Left: TMDMOC. Right: VCU.

2) Measurements: Following the approach adopted in our previous work on an ICE vehicle reported in [9], we performed channel measurements between all access points by means of a 2-port Vector Network Analyzer (VNA) in the frequency range of 100 kHz to 100 MHz, which is the frequency range typically considered for (in-vehicle) PLC (see overview in [12, Figure 1]). This approach provides frequency dependent scattering parameters that fully describe the transfer function between connection points as well as their access impedances. The measurements were repeated for the following different states: vehicle off, ignition switch on, combustion engine running at idle, and electrical mode with the rear traction wheels spinning on a roller type chassis dynamometer. Table I provides an overview of the measurements performed.

All connections were performed using the "VBAT" and "CHASSIS_GND" wires. To this end, custom made adapters were built to interface the VNA coaxial test cables with the on-vehicle connectors at the selected access points such that we could: a) connect in parallel to the power network without disconnecting any loads from the harness; b) selectively disconnect loads, to measure load impedance or the network without the load. Thus, this approach enables us to fully describe the transmission characteristics of the PLC network.

3) Connectors: Figure 2 shows the adapters built for the TMDMOC and VCU access points. All adapters are basically patch connections that are inserted at the junction of two (male/female) vehicle connectors. A coaxial connector in shunt with "VBAT" and "CHASSIS_GND" provides the access for the VNA test port. When commercially available end-launch connectors were used and mounted directly on the PCB board, when not, cable crimped connectors were used and the cables soldered to the PCB board. Given the high density of the end launch connectors and the high current ratings of the signals being patched the boards were designed to sustain up to 4 amps current at a 100°C temperature raise when fabricated with 3 oz copper thickness.

III. Measurement Results and Discussion

Figure 3 (top) shows the representation of a vehicular PLC system. The Thévenin equivalent circuit of the transmitter is linked via a two-port circuit representing the vehicle wiring to the load impedance representing the receiver. The two-port circuit is described by its S-parameters measured with the VNA and the reference impedance, which in our measurements was selected as $Z_0 = 50\ \Omega$. Given the S-parameters, the transfer

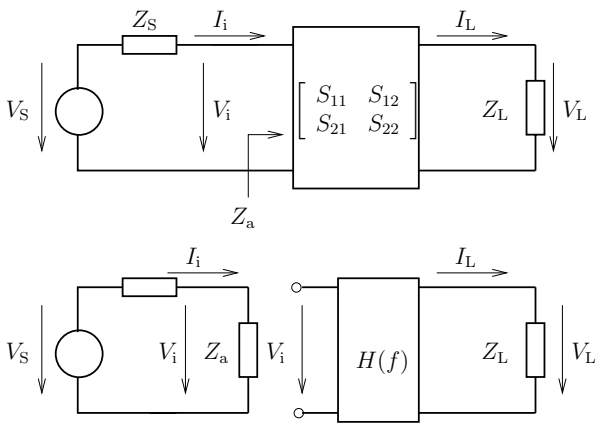

Fig. 3: Top: Vehicular PLC as two-port network. Bottom: Equivalent model.

function

$$H(f) \triangleq V_{\mathrm{L}}(f)/V_{\mathrm{i}}(f) = \frac{S_{21}(f)(1+\Gamma_{\mathrm{L}}(f))}{(1-S_{22}(f)\Gamma_{\mathrm{L}}(f))(1+\Gamma_{\mathrm{i}}(f))} \tag{1}$$

and the access impedance

$$Z_{\mathrm{a}}(f) = Z_0 \frac{1+\Gamma_{\mathrm{i}}(f)}{1-\Gamma_{\mathrm{i}}(f)} \tag{2}$$

can be obtained, where

$$\Gamma_{\mathrm{i}}(f) = S_{11}(f) + \frac{S_{21}(f)\Gamma_{\mathrm{L}}(f)S_{12}(f)}{1-S_{22}(f)\Gamma_{\mathrm{L}}(f)},\ \Gamma_{\mathrm{L}}(f) = \frac{Z_{\mathrm{L}}-Z_0}{Z_{\mathrm{L}}+Z_0} \tag{3}$$

and f denotes frequency. The transfer function $H(f)$ and access impedance $Z_{\mathrm{a}}(f)$ lead to the equivalent transmission model in Figure 3 (bottom), which is of interest for communications engineers.

We note that if $Z_{\mathrm{L}} = Z_0$, then $H(f) = S_{21}(f)$ and $Z_{\mathrm{a}}(f) = Z_0(1+S_{11}(f))/(1-S_{11}(f))$. In the following, we show results for $S_{21}(f)$ and $Z_{\mathrm{a}}(f)$ under the assumption of $Z_{\mathrm{L}} = Z_0$, as provided by the VNA.

A. Channel Transfer Function

1) Different Links: We first consider the vehicle in the off-state and compare the channel transfer function for different node-to-node links.

Figure 4 shows the magnitude transfer function ($|S_{21}(f)|$) as function of frequency f for transmission links from the VCU. These links seem to be particularly relevant as the VCU is the central control unit. We observe that the channel is fairly frequency selective, which is consistent with measurements for ICE and electric vehicles in e.g. [7], [9], [10], [13]. It can also be seen that attenuation is strongly link-dependent. The VCU-ESS and VCU-Relay links experience much less attenuation than the VCU-TMDMOC and VCU-DC/DC links, especially for frequencies below 50 MHz (note that all subplots in Figure 4 show the same y-axis range). Interestingly, the VCU-TMDMOC and VCU-DC/DC links are notably longer than the VCU-ESS and VCU-Relay links, which suggests a distance-proportional attenuation. This is further confirmed considering the results in Figure 5 for the links from the DC/DC converter.

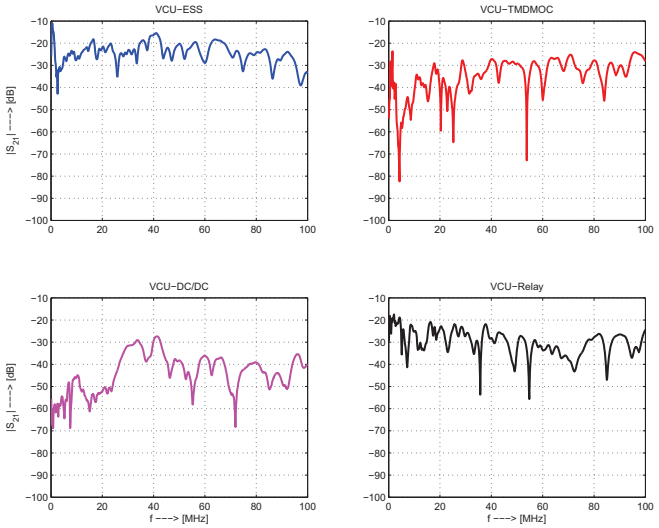

Fig. 4: Magnitude of $S_{21}(f)$ as function of frequency f for connections from VCU.

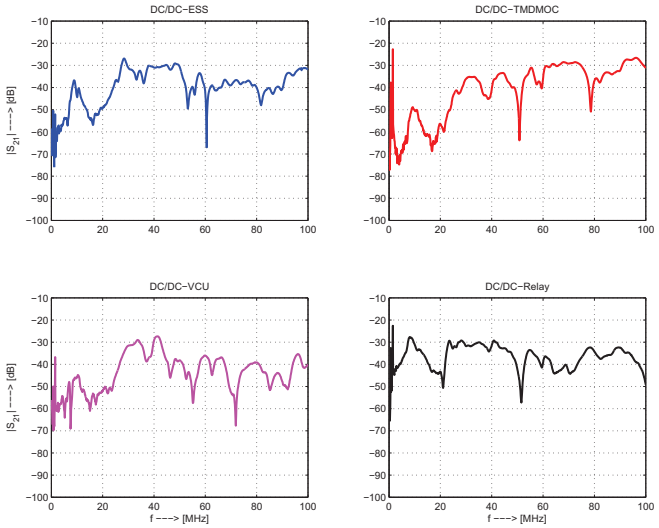

Fig. 5: Magnitude of $S_{21}(f)$ as function of frequency f for connections from DC/DC converter.

All links experience relatively high attenuation. The DC/DC-TMDMOC is the longest link and shows the smallest gain $|S_{21}(f)|$ for frequencies below about 50 MHz. The larger gains for higher frequencies could be due to frequency-dependent network impedances, which dominate attenuation, and parasitic wireless transmission. In this context, we also note that the 12V wires connecting the battery with VCU and TMDMOC run in the same cable bundle for some distance, which may lead to cross-talk and could explain the larger channel gain for VCU-TMDMOC compared to VCU-DC/DC seen in Figure 4.

Comparing the absolute attenuations with those for ICE vehicles, e.g., [7], [9], [10], and the EV in [13], we find them to be quite similar with the exception of the high attenuation of the links to/from the DC/DC and TMDMOC nodes at lower frequencies. This could be caused by low impedances of these loads at lower frequencies.

Finally, comparing the plots for VCU-DC/DC and DC/DC-VCU in Figures 4 and 5, the channels can be identified as reciprocal. This has been confirmed for all links that we measured.

2) Different Vehicle States: We now compare the transfer function results when operating the vehicle in different states. First, we consider the TMDMOC node, as it is connected to the 12V network through relay K6 (see Figure 1). The relay is open in the "off" state and closed in the "ignition" state. Figure 6 shows the channel gain $|S_{21}(f)|$ for both states. The changes in the channel gain due to the vehicle-state transition are overall not dramatic. This suggests that the high-frequency signal passes or bypasses the relay through parasitic capacitances.

Figure 7 presents the $|S_{21}(f)|$ for the three different vehicle states vehicle off ("off"), ignition switch on ("ignition"), and combustion engine idling ("idle, comb.") and for the two connections VCU-TMDMOC and VCU-DC/DC. Again, the overall differences are not dramatic, but changes in the transfer function gain of 10 dB to 20 dB can occur in certain frequency ranges. For example, considering the VCU-DC/DC link and the frequency range below 10 MHz, we observe a drop by 10 dB when the ignition switch is on, which could be caused by load changes when loads become powered.

Some notable effects occur when the electrical drive system is operating. This is highlighted in Figure 8, which compares $|S_{21}(f)|$ when the vehicle is off ("off") and it drives in the electrical drive mode ("spinning, elect."). Note that the frequency range from 100 kHz to 20 MHz is focused on in Figure 8. In the electrical drive mode, the frequency responses have many sharp peaks and notches, not present in the off-mode. We further observed that those change with time (which cannot be seen from the figure, of course). This suggests the

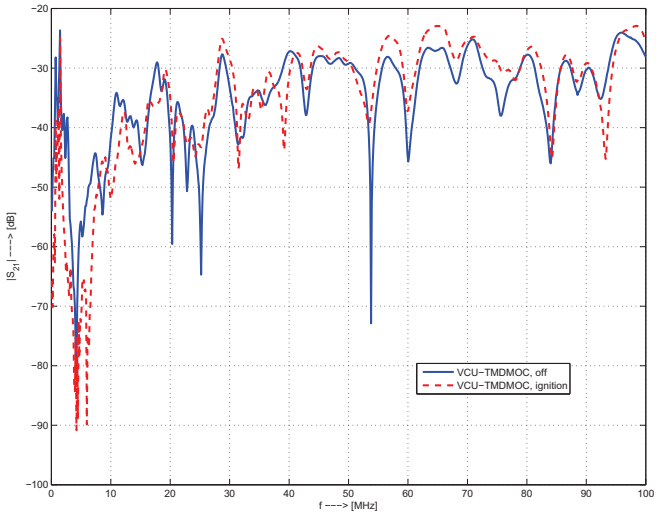

Fig. 6: Magnitude of $S_{21}(f)$ as function of frequency f for VCU-TMDMOC connection in different vehicle states: vehicle off ("off") and ignition switch on ("ignition").

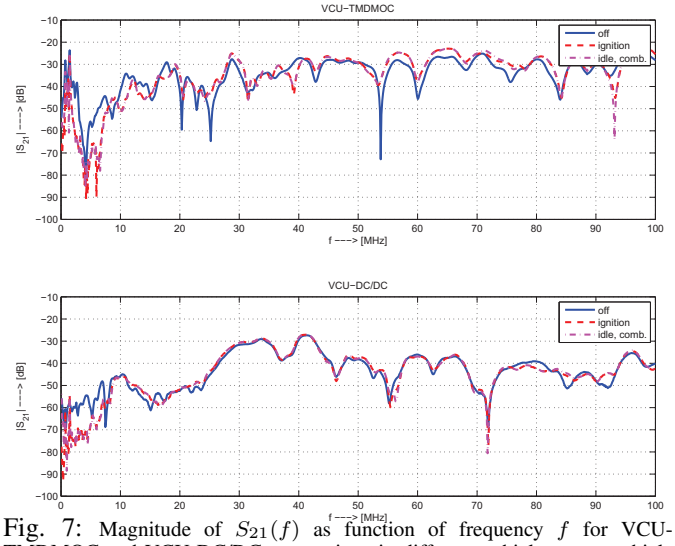

Fig. 7: Magnitude of $S_{21}(f)$ as function of frequency f for VCU-TMDMOC and VCU-DC/DC connections in different vehicle states: vehicle off ("off"), ignition switch on ("ignition"), combustion engine idling ("idle, comb.").

presence of an independent signal source in the network, i.e., noise induced into the network through loads, and/or the variation of load characteristics over time. Both would affect the VNA measurements. Preliminary noise measurements show an increased noise level in the range below about 15 MHz, which would be consistent with the observations from Figure 8. But further studies on noise and load-impedance characterization are needed (and ongoing) to fully explain this result.

B. Access Impedance

We now proceed to examine the access impedance Z_{a} obtained at each of the five selected access points on the HEV. The values obtained here add to our previous work for an ICE vehicle reported in [9], [12] and provide essential information for the design of prospect matching circuits.

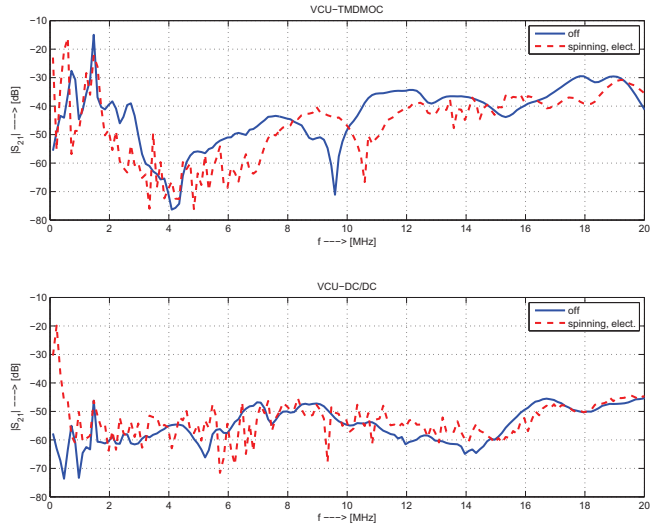

Fig. 8: Magnitude of $S_{21}(f)$ as function of frequency f for VCU-TMDMOC and VCU-DC/DC connections in different vehicle states: vehicle off ("off") and wheels spinning in electrical mode on a dynamometer ("spinning, elect.").

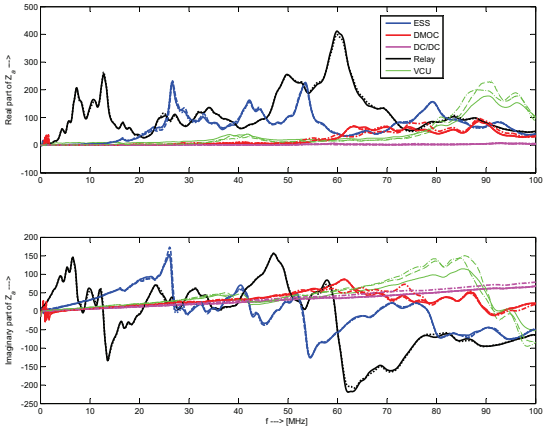

Fig. 9: Measured access impedances Z_{a} for different vehicle states. Top: real part, bottom: imaginary part. Solid lines are for vehicle off, dotted lines for ignition on, dashed for combustion engine idling, and dash-dot for wheels spinning in electrical mode on a dynamometer.

1) Obtaining the Access Impedance Z_{a}: In consistence with [12], we consider as access impedance Z_{a} the impedance seen by a PLC device connected in parallel to a PLC access point; e.g. for an access point located in the vicinity of a load, Z_{a} includes the effect of that load's impedance in parallel with the impedance seen towards the vehicle harness. Given that our test adapters allow for VNA measurements without disconnection of the loads, we calculated the corresponding access impedances directly from the measured scattering reflection parameter S_{11} using Eq. (2). It is important to note that no de-embedding of the adapters was performed at this stage, but that given their short physical dimensions we do not expect their phase insertion or loss to be of any significance in comparison to those of long networks being measured across. However stand alone characterization of the adapters has shown the presence of a resonance effect between the pins of the ESS automotive patch connectors, whose effect on the measurements needs to be further investigated. All other adapters were found resonant free and can be de-embedded by a simple port or electrical extension.

2) Measured Access Impedances: In Figure 9 we show the obtained Z_{a} for all access nodes and different vehicle states. The most noticeable features of these results are as follows. 1) There is very small influence of the vehicle state on the value of Z_{a}, with the sole exception of the VCU access point particularly at higher frequencies. 2) The high voltage battery node ESS, and the Relay have distinctively the widest impedance variations, but with the possibility that the measurements at the ESS node are affected by the connection adapter used during the measurements. 3) Z_{a} at the TMDMOC stands out as a purely inductive impedance with a small reactive and resistive components and at all vehicle states, which seems to indicate a small load impedance towards the TMDMOC.

From the perspective of a designer considering the requirements for a PLC impedance matching circuit it is essential

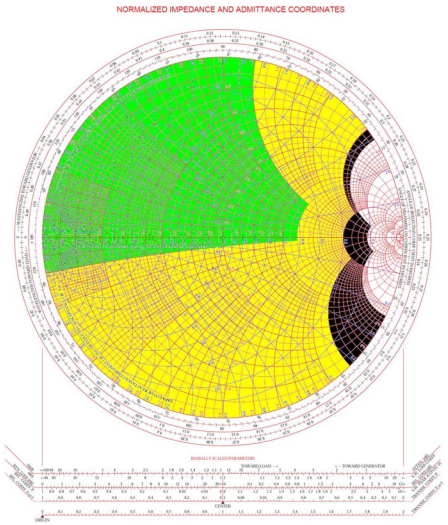

Fig. 10: Smith chart illustration of access impedance ranges according to measurement results. Coloured areas: Green: reduced frequency range of 30-40MHz. Green and yellow: average impedance values in the frequency range from 100 kHz to 100 MHz. Green-yellow-black: complete range of measured results.

to know the range of impedances to match to. To help visualize this range, Figure 10 shows the span of measured impedances on a Smith Chart normalized to $Z_0 = 50\ \Omega$. The regions colored in green, yellow, and black, altogether represent the complete range of measured Z_{a} for frequencies between 100 kHz and 100 MHz. Combined regions colored in green and yellow are for possible average values if ignoring the isolated large peak variations that correspond to the black area, such as for example those occurring at 60 MHz on the Relay as shown in Figure 9. To illustrate the value of this information, the region colored in green shows the range of impedance variations if the PLC system is designed to operate in this vehicle in the range of 30 MHz to 40 MHz. As it is seen, this area is very smaller than the total area to be covered. In the other words, there is a smaller range of impedance that should be matched by impedance matching system. This casts less restriction on the impedance matching circuit designer in both term of structure and elements necessary to address this need.

IV. Conclusion

V-PLC is an appealing approach for communication in vehicles, especially EVs, for it reduces complexity, size, and weight of the wiring harness. Since there are very little results on channel characteristics for V-PLC in EVs known, in this paper we have presented and discussed results for transfer function and access impedance from a measurement campaign for an HEV. We hope that a methodology similar to what has been presented here can be adopted by other research groups, leading to a broader basis of measurement results and thus better understanding of the channel characteristics. Furthermore, to enable the reader to work with our measurement results beyond what we have presented here, we have made the measurements available at http://www.ece.ubc.ca/~lampe/VehiclePLC_folder/PLC.htm. To complete the picture and gain an understanding of what performance is achievable with V-PLC, our ongoing investigations focus on noise measurements in the HEV.

Acknowledgment

The authors would like to thank Azure Dynamics Corporation, Vancouver Office, for their excellent support of the measurement campaign.

References

[1] Strategy Analytics Automotive Electronics report, November 2007, "Automotive Multiplexing Protocols: Cost/Performance Driving New Protocol Adoption," cited from http://www.businesswire.com/news/home/20071115006121/en/STRATEGY-ANALYTICS-Automotive-Electronics-Network-Market-Stretch, accessed on August 28, 2011.

[2] H. Ferreira, L. Lampe, J. Newbury, and T. Swart, *Power Line Communications: Theory and Applications for Narrowband and Broadband Communications over Power Lines*. John Wiley & Sons, Ltd., Jun. 2010.

[3] F. Nouvel, G. El Zein, and J. Citerne, "Code division multiple access for an automotive network over power lines," in *IEEE Vehicular Technology Conference (VTC)*, Jun. 1994, pp. 525–529.

[4] Y. Maryanka, "Wiring reduction by battery power line communication," in *IEE Seminar on Passenger Car Electrical Architecture*, Jun. 2000, pp. 8/1–8/4.

[5] A. Schiffer, "Statistical channel and noise modeling of vehicular dc-lines for data communication," in *IEEE Vehicular Technology Conference (VTC)*, Tokyo, Japan, May 2000, pp. 158–162.

[6] W. Gouret, F. Nouvel, and G. El-Zein, "Powerline communication on automotive network," in *IEEE Vehicular Technology Conference (VTC)*, Apr. 2007, pp. 2545 – 2549.

[7] M. Lienard, M. Carrion, V. Degardin, and V. Degauque, "Modeling and analysis of in-vehicle power line communication channels," *IEEE Trans. Veh. Technol.*, vol. 57, no. 2, pp. 670–679, Mar. 2008.

[8] V. Degardin, M. Lienard, P. Degauque, E. Simon, and P. Laly, "Impulsive noise characterization of in-vehicle power line," *IEEE Trans. Electromagn. Compat.*, vol. 50, no. 4, pp. 861 –868, Nov. 2008.

[9] M. Mohammadi, L. Lampe, M. Lok, S. Mirabbasi, M. Mirvakili, R. Rosales, and P. van Veen, "Measurement study and transmission for in-vehicle power line communication," in *IEEE International Symposium on Power Line Communications and Its Applications (ISPLC)*, Apr. 2009, pp. 73 –78.

[10] A. Vallejo-Mora, J. Sánchez-Martínez, F. Cañete, J. Cortés, and L. Díez, "Characterization and evaluation of in-vehicle power line channels," in *IEEE Global Telecommunications Conference (GLOBECOM)*, Dec. 2010, pp. 1 –5.

[11] Y. Yabuuchi, D. Umehara, M. Morikura, T. Hisada, S. Ishiko, and S. Horihata, "Measurement and analysis of impulsive noise on in-vehicle power lines," in *IEEE International Symposium on Power Line Communications and Its Applications (ISPLC)*, Mar. 2010, pp. 325 –330.

[12] N. Taherinejad, R. Rosales, S. Mirabbasi, and L. Lampe, "A study on access impedance for vehicular power line communications," in *IEEE International Symposium on Power Line Communications and Its Applications (ISPLC)*, Udine, Italy, Apr. 2011, pp. 440 –445.

[13] S. Barmada, M. Raugi, M. Tucci, and T. Zheng, "Power line communication in a full electric vehicle: Measurements, modelling and analysis," in *IEEE International Symposium on Power Line Communications and Its Applications (ISPLC)*, Mar. 2010, pp. 331 –336.

[14] E. Bassi, F. Benzi, L. Almeida, and T. Nolte, "Powerline communication in electric vehicles," in *IEEE International Electric Machines and Drives Conference (IEMDC)*, May 2009, pp. 1749 –1753.

[15] Yamar Electronics, "Yamar DCB500 Transceiver for Powerline Communication," http://www.yamar.com/datasheet/PO-DCB500.pdf, Accessed on November 25, 2011.

[16] "BalanceTM Hybrid Electric Vehicle Owners Guide Supplement 2011 Ford E-450," http://www.azdtec.com/techlibrary/balance/OG/BHEV_OGS_0211_RO.pdf.

[17] "Balance Hybrid Electric Vehicle Specifications and Ordering Guide 2011/2012," http://www.azuredynamics.com/products/SPC500985-B.pdf.pdf.

[18] "AZDtec Dealer Support Solutions," http://azdtec.com.